Supporting Information

Activity of Tumor Necrosis Factor α is Modulated by Dynamic Conformational Rearrangements

Daniela Hofmann, Loïc Salmon, Gerhard Wider*

Institute of Molecular Biology and Biophysics, ETH Zürich, 8093 Zürich (Switzerland)

Supporting Methods

Protein Expression and Purification: The cDNA encoding human N-terminal $(His)_6$-tagged TNFα (UniPortKB – P01375, residues 6-157), was cloned into pET-23a vector (Novagen) and transformed into BL21-CodonPlus (DE3)-RIL competent cells (Agilent) for expression. Mutants (T89A, T72A, I97A, L57Y, G121A, Y59A, Y119S) were constructed by Quick-change™ site-directed mutagenesis. $(His)_6$-TEV-tag TNFα was constructed by cloning human TNFα (residues 6-157) between Xho1 and BamH1 restriction sites of the pEM1 vector (gift from Dr. Erich Michel, University of Zurich, Zurich). Protein production was performed as previously described [1]. ^{15}N-labeled TNFα was expressed in M9 minimal media (8.5 g $Na_2HPO_4.2H_2O$, 3 g KH_2PO_4, 0.5 g NaCl, 2 mM $MgSO_4$, 1 g $^{15}NH_4Cl$ (98 atom% ^{15}N, CIL), 10% (v/v) vitamin mix (Sigma), 2 mM trace elements (self made), 50 mg antibiotics, 2% glucose for ^{15}N only / 0.4% ^{13}C-glucose (99 atom%, U-$^{13}C6$, CIL) for ^{13}C labeling, pH = 7.2) For the production of perdeuterated [^{13}C, ^{15}N]-labeled TNFα, clones were grown on Lysogeny Broth (LB)-D_2O plates prior to pre-culture. The minimal media was enriched with ^{2}H-^{13}C-glucose (U-$^{13}C6$, 99%, 1,2,3,4,5,6,6-D7, 97-98%, CIL) and using 98% D_2O instead of H_2O. Mutant TNFα versions were produced in minimal media enriched with 1 g $^{15}NH_4Cl$ (98 atom% ^{15}N, CIL). Expression of single amino-acid type (Cys, Arg, Lys, or Asn) unlabeled TNFα in an otherwise uniformly ^{15}N- and ^{13}C-labeled background was achieved by addition of 1 g/L of the specific natural abundance ^{14}N-, ^{12}C-amino-acid to the cell culture prior to induction as previously described [2]. Protein purity and molecular weight was confirmed by Mass spectrometry and the activity of TNFα verified by cytotoxicity assay using mouse fibroblast cells (LM, ATCC®) [3]. The protein lacks the N-terminal Met and is acetylated. The N-terminal $(His)_6$-tag was shown not to influence the structure, as evidenced by a perfect overlap of 1D ^{1}H and 2D [^{1}H, ^{15}N]-HSQC spectra of TNFα with and without $(His)_6$-tag, nor does it influence drug binding to SPD304 as evidenced by alike spectra after addition of the inhibitor.

NMR Spectroscopy and Assignment:

Specifications of the spectrometers used (Bruker Biospin, Karlsruhe, Germany)

Field	*Console*	*Probe head*
500 MHz	AVIII	Cryo Probe TCI Z44881/008
600 MHz	AVIII	Cryo Probe CPQCI Z109742/0016
600 MHz	AVIII HD	Cryo Probe CPTCI Z129649/0014
700 MHz	AVIII	Cryo Probe CPTCI Z-GRD Z44908/54
750 MHz	AVIII	PATXI (ATM) Z830901/007
900 MHz	AVIII HD	Cryo Probe CPTCI Z107926/0001

Sequence specific backbone resonance assignment was obtained on a 1 mM uniformly [^{2}H, ^{13}C, ^{15}N]-isotope-labeled TNFα dissolved in 100 mM PBS, pH 7.4, using a set of two dimensional (2D) [^{15}N,^{1}H] transverse relaxation optimized (TROSY) and [^{13}C,^{1}H] heteronuclear single quantum coherence (HSQC) spectra as well as TROSY versions of three-dimensional (3D) HNCO, HN(CA)CO, HN(CO)CA, HNCACB, HN(CO)CACB and a ^{15}N-resolved [^{1}H, ^{1}H]–NOESY (mixing time τ_m=120 ms) spectra. Spectra were recorded on 600, 700, or 900 MHz NMR spectrometers at 310 K. [^{1}H, ^{15}N]-HSQC and 3D HNCO spectra of TNFα produced with Arg, Lys, Cys, and Asn specific unlabeling schemes were measured at 600 MHz (Cys, Arg HSQC at 750 MHz, and Asn HNCO at 500 MHz). Based on the unlabeling strategy, the correct assignment of the amino acid type could be confirmed for residues K11, N30, N39, N46, K65, N92, K98, C101, R103, K112, K128, R131, N137, R138 in [^{1}H, ^{15}N]-HSQC spectra. Measurements of [^{1}H, ^{15}N]-HSQC spectra of mutant TNFα were conducted at 600 MHz (G121A, Y119S, T89A, T72A, I97A) and 700 MHz (Y59A, L57Y, Y119S). Site-directed mutagenesis confirmed residues T72, T89, I97, I155 and neighboring residues. With this combinatory approach 98.4% of all visible and 83.3% of all expected resonances in a [^{1}H, ^{15}N]-TROSY spectrum could be assigned. All identified amide [^{1}H-^{1}H]-NOEs are consistent with the tertiary structural features of the published TNFα crystal structure [4]. Notably, three measured NOEs correspond to distances in the crystal structure larger than the usually expected 5 Å (V13–V41 6.1 Å, S85–E131 5.79 Å, F64–L142 5.8 Å) but can be explained by prolonged β-strands D and B' by one residue, consistent with secondary chemical shifts and results of the proton/deuterium (H/D) exchange experiment.

NOESY Spectra: [^{1}H,^{15}N,^{1}H]-NOESY experiments of the mutant TNFα Y119S were conducted on a 500 µM sample in 150 mM MOPS, 50 mM ammonium acetate, pH 7.2 at 600 MHz, collecting 16 transients. Spectra for the complex TNFα:SPD304 at a molar ratio (1:0.75) were obtained on a 400 µM TNFα using the same buffer on a 700 MHz spectrometer, collecting 16 transients. Spectra were compared to TNFα recorded on a 1.5 mM TNFα sample in 100 mM PBS buffer, pH 7.4 at 700 MHz, collecting 8 transients. All spectra were processed in the same way to obtain maximal evolution times of 60 ms, 10 ms and 10 ms in the ^{1}H, ^{15}N and ^{1}H (NOE) dimension, respectively, zero filling to 2048(t_3), 128(t_2) and 512(t_1) data points was applied.

Combined Chemical Shift Deviations (CCSD): ^{13}C CCSD were computed as the difference between C^{α} and C^{β} secondary chemical shift, i.e. their deviation from the random coil shifts, as described [5].

H/D Exchange Experiments (700 MHz): a 280 µM ^{15}N-labeled TNFα sample was lyophilized overnight and quickly dissolved in 100% D_2O right before measuring. Changes in signal intensities were monitored by 2D [^{1}H, ^{15}N]-HSQC spectra in the period 10 min after dissolution to 17 days. The time dependent intensity (signal height) was fitted using "Dynamic Centre" (Bruker, Karslruhe, Germany). Fast and slow exchanging amide protons are distinguished based on the remaining fitted intensities 2 h post dissolution.

^{15}N Relaxation (T_1,T_2, and hetNOE) of TNFα: ^{15}N spin relaxation measurements were performed on a ^{15}N-labeled 1.2 mM sample in 150 mM MOPS, 50 mM ammonium acetate, pH 7.2 at 700, 600, and 500 MHz. The sets of the three relaxation experiments were measured with the following parameters for the three magnetic fields 500/600/700 MHz. An acquisition time of 0.0466/0.0365/0.0466 s in the indirect and 0.106 s in the direct dimension and a relaxation delay of 1/5/1 s for T_1 and 1/3/1 s for T_2, 7 s for the saturated $\{^1H\}-^{15}N$ heteronuclear nuclear Overhauser effect (hetNOE) and 10 s for the reference hetNOE experiment were used. T_1 experiments accommodate selective proton and water flip back pulses. For the T_1 measurements 40/32/40 scans per t_1 increment were done and 8 experiments recorded, in an interleaved manner, with the following randomly ordered relaxation delays: 0.1, 0.2, 0.4, 0.7, 0.9, 1.6 and 3.3 s (in the order 5-2-4-3-6-2-7-1). T_2 measurements were conducted using a sequence employing a CMPG pulse scheme with an echo delay of 500 µs between two successive 180° pulses. In total 5 different relaxation delays were recorded: 0, 18.2, 36.5, 54.7, 72.9 ms, (in the order 3-1-5-2-4-3) with 40, 24, and 40 scans at 500, 600, and 700 MHz, respectively. Duplicates of at least one relaxation time were done for all experiments for error estimations. For the NOE experiments a slightly modified version of the sequence described by Farrow was used [6]. The experiment was run in an interleave manner and employed water flip back pulses. The saturation of the ^{1}H was achieved by applying a series of 120° pulses for 3 ms following a recycling delay of 7 s. 64 scans were accumulated. All spectra were Fourier transformed with base line correction. The data were analyzed using the software "Dynamic Centre" (Bruker, Karslruhe, Germany). Peaks pairs closer than 0.06 ppm and 0.6 ppm in the direct and indirect dimension, respectively, were excluded due to possibly biased peak intensities. The longitudinal and transverse relaxation times were determined from fitting the intensity changes as a function of the relaxation delays, I(t), for every resonance according to $I(t) = I(0)\exp(-t/T)$. Intensity errors were estimated based on the noise level in the NMR spectra. Final errors were derived from Monte Carlo simulation, and errors from duplicated measurements were within these errors. The steady-state NOEs were determined from the ratio (I_{NOE}/I_{REF}) between the intensities obtained in the two interleaved spectra with and without saturation of the amide proton spins. The errors in NOE (σ_{NOE}) were calculated according to $\sigma_{NOE} = NOE * \sqrt{\left(\frac{N_{NOE}}{I_{NOE}}\right)^2 + \left(\frac{N_{REF}}{I_{REF}}\right)^2}$, where N is the noise level and I the intensity of the considered resonance.

The global correlation time, assuming isotropic tumbling, was estimated based on the ratio R_2/R_1 according to $\tau_c = \frac{1}{4\pi\nu_N}\sqrt{6\frac{R_2}{R_1} - 7}$ [7] for the 40% trimmed mean (which discards lowest and highest 20% of values) representing the most rigid residues. Correlation times of 24.1 ns, 25.1 ns, and 25.6 ns were obtained for measurements performed at 500, 600, and 700 MHz, respectively, compatible with a trimer.

Model-free analysis and determination of the anisotropic diffusion tensor was performed using Tensor v2.0, implementing multiple field analysis [8]. ^{15}N R_1, R_2, and hetNOE values measured at 500, 600, and 700 MHz were analyzed successively and simultaneously. Residues with a hetNOE value larger than 0.7 and forming regular secondary structure based on the crystal structure [4] were chosen for fitting the diffusion tensor. Generalized order parameters were obtained using single and multiple

field strengths for all residues with determined ^{15}N-spin relaxation as described by Lipari & Szabo [9–11]. Values describing the rotational diffusion tensor determined from fitting experimental R_2/R_1 values from all three fields are as follows:

	D_x (10^6 s^{-1})	D_y (10^6 s^{-1})	D_z (10^6 s^{-1})	α (°)	β (°)	γ (°)
TNFα	5.90±0.24	6.07±0.17	6.90±0.24	-74.0±43.4	52.1±17.9	-44.4±24.2

Cross-Correlated Relaxation: The dipole-dipole (DD)/ chemical shift anisotropy (CSA) cross-correlation constants (η_{xy}) were measured using a sequence from Tjandra et al. [12] yielding two spectra differently modulated by the cross-relaxation effects (I_A, I_B). NMR experiments were performed at 700 MHz using a sample of 1.2 mM TNFα and a sample of 0.4 mM complex TNFα:SPD304 (1:0.75). A total of 32 scans, with acquisition times and complex data points of 36 ms / 140 (t_1) and 91 ms / 2 k (t_2) was collected. The inter-scan delay was 3 s and the duration of the relaxation delay (Δ) was 5 ms or 7 ms. The experiments were repeated twice for each relaxation delay. For free TNFα two additional experiments with (Δ = 4 ms, Δ = 6 ms) were conducted. The ratio of the intensities (I_A/I_B) of the cross peaks, were obtained from peak height and fitted according to $I_A/I_B = \tanh(2\Delta\eta)$. The standard error of the nonlinear fit was estimated based on the residuals of the fit. Only resolved resonances where the η_{xy} could be determined with high confidence (for free TNFα, resonances closer than 0.06 ppm and 0.6 ppm in the direct and indirect dimension, respectively, were excluded due to biased peak intensities; for the complex, resonances 22-24, 29, 39, 43, 46, 47, 53-54, 68-76, 78, 84, 86-87, 90, 92, 107-109, 111-112, 126, 128-132, 138, 140, 142, 145) and a standard error < 15% were considered.

2D [^{15}N, ^{1}H]- and [^{13}C, ^{1}H]-HSQC Titration of SPD304 to TNFα: SPD304 was titrated stepwise to 500 µL of 230 µM [^{13}C, ^{15}N]-labeled TNFα in 150 mM MOPS, 50 mM ammonium acetate, pH 7.2. Four titration steps were conducted and in every step 3.3 µL of a 12 mM stock solution of SPD304 in 100% DMSO-d_6 were added. Spectra were measured at 600 MHz at 310 K. The resulting concentrations for TNFα, SPD304, and DMSO-d_6 are summarized below. The concentration of the SPD304 stock solution and the amount of soluble SPD304 at each titration point was further estimated using PULCON [13]. The relative amount of SPD304 added in each titration point was double-checked based on the residual DMSO-d_6 proton signal at 2.52 ppm. A maximal deviation of 8% was obtained. The influence of DMSO-d_6 on TNFα was verified by adding DMSO-d_6 to an identical TNFα sample and measuring the same spectra as for the titrations. No influence on DMSO-d_6 on the chemical shifts or intensities of TNFα was observed up to concentrations of 2.5% (v/v) DMSO-d_6. The pH was stable over the whole titration, as verified by addition of 1 mM $KPHO_4$ to the protein sample, to be able to observe chemical shifts of the pH sensitive phosphate signal by ^{31}P NMR at every time point. The removal of the N-terminal $(His)_6$-tag did not influence ligand binding.

Titration step (Ratio SPD304/TNFα)	[TNFα] (mM)	[SPD304] ± err (mM)	[DMSO-d_6] (%)
Free TNFα	0.230	-	-
1 (0.3)	0.230	0.080 ± 0.006	0.65
2 (0.7)	0.230	0.160 ± 0.012	1.29
3 (1.0)	0.220	0.230 ± 0.018	1.90
4 (1.4)	0.220	0.300 ± 0.023	2.47

Combined Chemical Shift Perturbation: Combined ^{1}H and ^{15}N chemical shift perturbation ($\Delta\delta$) from titrations were obtained using the following equation, with a scaling factor α of 0.15 [14]:

$$\Delta\delta = \sqrt{\frac{1}{2}\left(\Delta\delta_H^2 + \alpha\Delta\delta_N^2\right)}$$ with $\Delta\delta_H$ and $\Delta\delta_N$ being the respective chemical shift changes for ^{1}H and ^{15}N (Figure S2).

Changes of Resonance Intensities upon Perturbation of the Protein-Protein Interface (PPI): [^{1}H, ^{15}N]-HSQC spectra were measured for all titration steps and for the mutants G121A, Y59A, Y119S, T89A, T72A, I97A, and L57Y. The spectra were analyzed and cross peaks heights were extracted using the program CARA 1.8.4 (cara.nmr.ch, Switzerland). Pairs of resonances closer than 0.06 ppm and 0.6 ppm in the direct and indirect dimension, respectively, were excluded to avoid possible biased intensities. Resonance frequencies were adjusted to the peak maxima using CARA in every spectrum within the range of 0.06 ppm and 0.4 ppm in ^{1}H and ^{15}N dimension, compared to free TNFα. The resonance intensities for the mutants (G121A, Y59A, Y119S, T89A, T72A, I97A, and L57Y) were scaled for equal signal-to-noise ratio (S/N) of the resolved, most upfield shifted Asn/Gln NH_2 side chain resonance (7.145 ppm / 109.292 ppm), which allows for comparable quantification of the intensity changes. The rate of the decrease of the cross peak intensity for the titration with SPD304 was obtained using the software "Dynamic Centre" (Bruker, Karslruhe, Germany) by fitting the intensity decrease (change in signal height), with successive titration steps using $I[SPD304] = I_0 \cdot \exp(-[SPD304]/K)$, with K being the intensity decrease constant.

TROSY for Rotational Correlation Time (TRACT) Measurements: TRACT experiments were acquired on 750/600 MHz spectrometers, respectively. 48/112 relaxation rates (t_{Rmax} = 100/170 ms), with 160/144 transients were recorded. An inter-scan delay of 1.5 s was used. The spectra were Fourier transformed and base line corrected. The integral of the 1D ^{1}H spectra over the spectral region from 6.2 ppm to 11.0 ppm (at 600 MHz from 7.2 ppm to 9.4 ppm due to T1 noise) was then measured as a function of the different ^{15}N relaxation delays (Δ). Fitting of the intensity (I) decay for both the fast and slowly relaxing spin states was performed according to $I_{\alpha/\beta}(\Delta) = I_o.\exp(-R_{\alpha/\beta}.\Delta)$, yielding two relaxation rates, R_α and R_β, for the two spin states α and β of the ^{15}N nucleus, respectively. The effective rotational correlation times, τ_c, were calculated according to $R_\beta - R_\alpha = 2\eta_{xy} = 2p\delta_N[4J(0) + 3J(\omega_N)](3\cos^2\theta - 1)$ with the spectral density function $J(\omega) = 0.4\tau_c / [1 + (\tau_c\omega)^2]$ [15]. The following values were used: a ^{1}H-^{15}N inter-nuclear distance r_{HN} = 1.02 Å, an angle of $\theta = 17°$ between the ^{15}N chemical shift tensor and the NH bond, and a ^{15}N-CSA of $\Delta\gamma_N$ = 160 ppm [16]. The protein concentrations were 230 µM for TNFα and TNFα:SPD304 (1:1.14) and 600 µM for TNFα and Y119S.

Quenched H/D Exchange Experiments: Two TNFα samples (500 µM ^{15}N-labeled TNFα in 150 mM MOPS, pH 7.2) were lyophilized and dissolved in D_2O. For one sample SPD304 was added to a final concentration of 300 µM, 2.5% DMSO-d_6, to the other DMSO-d_6 was added in equal amounts. Half of each sample was kept for 10 min (t_1), the other half for 4 h (t_2) at room temperature. The reaction was quenched by lowering the temperature to 4 °C. All samples were further buffer exchanged to 150 mM MOPS, pH 7.2 in D_2O at low temperature (4 °C) using Amicon-ultra-10k®. In total, the samples dialyzed against 27,000-times their volume over a time period of 12 h, which was sufficient to fully remove SPD304. Subsequently [^{1}H, ^{15}N]-HSQC spectra were measured of the two quenched (t_1, t_2) and two ref (t_1, t_2) samples at 30 °C at 600 MHz (Figure S7).

Ultraviolet Circular Dichroism (UV CD): Optical activity was measured on a JASCO J-715 spectropolarimeter at 30 °C. Near UV spectra were acquired on a protein concentration of 300 µM using cuvettes with a path length of 1 cm. Either 2.5% DMSO or 300 µM SPD304 with a final concentration of 2.5% DMSO was added and the absorbance measured between 240 and 330 nm. 5 scans were averaged and a baseline subtraction was performed. The measurements were repeated two and three times on different preparations for TNFα and TNFα:SPD304, respectively, and averaged. All samples were filtered before use (22 µm, Millipore). TNFα was incubated with SPD304 for 1 h prior to the measurements. A mean weight for amino acids of 112.08 Da was taken to derive the mean residue ellipticity [17]. Far UV (200-250 nm) was measured using a 1 mm cuvette on a TNFα sample of 0.179 mg/mL and of a mutant TNFα sample Y119S of 0.427 mg/mL in 100 mM PBS, pH 7.4 buffer. Spectra were averaged over 5 scans and the baseline subtracted. The curves were subsequently smoothed. The near UV CD spectra, reporting on the tertiary structure, shows the typical TNFα "fingerprint" spectra (three maxima at 292.5, 285.5 and 280.5 nm), followed by two further shoulders at 278 nm and 267.5 nm as described in literature [18,19]. Perturbations of the interface by SPD304 binding reveal minor differences compared to the free TNFα: the main maxima are also present, however, slightly shifted from 292.5 nm to 294.5 nm and from 285.5 nm to 285-287 nm. Further, a decrease in dichroic absorption in the region 294.5 nm to 275 nm and an increase in the range 255 nm to 275 nm is apparent (Figure 5).

Biophysical Investigation of the Oligomeric State of TNFα: For multiangle light scattering (MALS), analytical ultracentrifugation (AUC), and dynamic light scattering (DLS), preparations of the complex were incubated 1 to 2 h at room temperature prior to measurements and samples filtrated (22 µM, Millipore) right before use (Figure S3).

Multi-angle Light Scattering: Size-exclusion chromatography (SEC) coupled to MALS measurements were performed on a 1.5 mg/mL TNFα sample and on a mixture of 90 µM TNFα and 300 µM SPD304 at 25 °C. The sample was resolved on a Thermo scientific Ultimate 3000 HPLC with a Superdex™ 200, 10/300 GL applying a flow rate of 0.5 mL/min. Scattering was measured using a Wyatt Technology instrument with a mini DAWN TREOS and Optilab T-rEX detectors (Figure S3).

Analytical Ultra-Centrifugation: AUC was performed on a 45 µM TNFα at 25 °C and on a mixture of 45 µM TNFα and 300 µM SPD304 with 45,000 rpm. The continuous C(s) distributions was determined using SEDfit [20]; values for solvent viscosity of $\eta = 1.002$ mPa s and density of $\rho = 1.0053$ g/mL were taken (Figure S3).

Dynamic Light Scattering: DLS experiments were performed on a 60 µM TNFα, L57Y, Y119S, and Y54A mutants as well as 60 µM TNFα:SPD304 (1:5). The samples were prepared in 100 mM PBS, pH 7.4, 2.5% DMSO-d_6. For determination of the hydrodynamic radius of TNFα, two different sample probes were measured and technical triplicates performed for each sample. DLS has been measured on a Zetasizer Malvern Instrument at 23 °C. Analysis of the data from the DLS detectors was performed using the MALVERN software V-7.03 (www.malvern.com) and scattered intensities analyzed by the method of CONTIN [21].

Size-Exclusion Chromatography: SEC using a Superdex™ 75 HR 10/300 column (GE Healthcare) was performed on an AEKTA Purifier (GE). 100 mM PBS, pH 7.4 was used as a running buffer. 70 µL of approximately 200 µM protein sample (native TNFα or mutant versions) was injected and a flow rate of 0.5 mL/min applied. The protein was monitored at 280 nm. The retention volume for TNFα at 300 µM in complex with SPD304 (1:1.4) was obtained using the same method, however the running buffer was changed to 150 mM MOPS, 50 mM ammonium acetate, pH 7.2.

Thermal Shift Assay (TSA) with SYPRO® Orange: The thermal stability of TNFα in presence or absence of SPD304 was assessed by measuring the SYPRO® Orange (Invitrogen) fluorescence intensity as a function of temperature between 10 °C and 95 °C using a BioRad CFX96™ Real Time System [22]. Excitation and emission of SYPRO® Orange are at 492 and 610 nm, respectively. 5 µL dye (1:16 diluted) was added to 45 µL 100 µM protein in 100 mM PBS, pH 7.2 buffer. Duplicates of each measurement were done. The melting temperatures (T_M) were determined by applying a first derivative of the fluorescence signal as a function of temperature (-dF/dT). Melting temperatures of 62 °C and 60 °C were obtained for TNFα and the Y119S mutant, respectively.

Nano-Electrospray Ionization Mass Spectrometry (nanoESI-MS): The experiments were conducted as previously described [1]. The following three protein samples were prepared: 4.5 µM TNFα and 4.5 µM TNFα:SPD304 (1:3) both in 75 mM ammonium acetate buffer (pH 7.7) with a final DMSO concentration of 1% (v/v), further 4.5 µM Y119S mutant in 75 mM ammonium acetate buffer (pH 7.7) (Figure S4).

MicroScale Thermophoresis (MST) with Fluorescein-tagged TNFα: TNFα was labeled with fluorescein isothiocyanate isomer I (Sigma) following standard protocols. The protein was purified by overnight dialysis against 2x 5 L 100 mM PBS, pH 7.4. The absorbance of the dye and the protein were measured at 494 nm and 280 nm, respectively, before the MST measurements. The MST data were recorded on a monolith NT.115 instrument using 40 % and 60 % MST power and ~20 % LED power. The buffer was 100 mM PBS, pH 7.4 complemented with 0.05% Tween-20 and a final DMSO concentration of 0.5%. Hydrophobic capillaries have been used. Fluorescein-tagged TNFα was kept constant at 0.5 nM and the change in fluorescence was recorded over increasing amounts of added unlabeled TNFα. The experiment was conducted in absence and presence of 600 nM SPD304. Duplicates of each measurement were performed at a temperature of 25 °C. For a course idea of an experimental error we used the averaged root mean squared deviation between the two repeated datasets (Figure S5).

Cross-linking: TNFα and TNFα:SDP304 present at different concentrations ranging from 1 nM to 10 mM have been cross-linked using 4-(4,6-Dimethoxy-1,3,5-triazin-2-yl)-4-methylmorpholinum chloride (DMTMM) and pimelic-d_{10} acid dihydrazide (PDH) according to the published protocol by Leitner et al [23]. Stock solutions of DMTMM and PDH were freshly prepared in 100 mM PBS, pH 7.4. The cross-linking samples were incubated at 37 °C for 4 to 6 h. The reaction was subsequently loaded on an SDS-PAGE gel and silver stained (Figure S6). For the *in vivo* experiments, the cross-linking reaction was quenched, cross-linker and initiator removed, and cross-linked trimetric TNFα as well as cross-linked TNFα:SPD304 purified by gel filtration (Superdex™ 75 10/300 GL). The buffer condition was adjusted to allow separating cross-linked trimeric TNFα forms from the remaining non-cross-linked trimeric TNFα forms (buffer condition: 100mM PBS, pH 7.4, 0.5% Tween 20, 0.2 M NaCl). Approximately 1-10% non-cross-linked TNFα remained in the cross-linked TNFα samples based on the size of the band at the molecular weight of the monomer versus the band at the molecular weight of the trimer on the SDS-PAGE gels (Figure S10).

8-Anilino-1-Naphthalenesulfonic Acid (ANS) Fluorescence: Fluorescence spectra were measured on a PTI Fluorometer between 400 nm and 600 nm with excitation at 380 nm at 30 °C. The following protein samples were prepared: 1.3 µM TNFα, 1.3µM TNFα and 6µM SPD304 and 6µM SPD304 in 50 mM ammonium acetate buffer, pH 7.6 as well as 1.3 µM TNFα, 1.3 µM Y119S, 1.3 µM Y59A, and 1.3 µM TNFα in presence of 1 M guanidinium chloride (GdmCl); ANS only at

400 µM served to establish the baseline of ANS fluorescence. As a negative control 8 M urea and 2 mM DTT were supplemented to the buffer described above. Spectra were measured twice and averaged. All buffers contained ANS at a 250 molar excess over protein concentration (Figure S8).

Trypsin Digestion: 0.04 mg/mL protein was mixed to 100:1 and 1000:1 (w/w) trypsin (Sigma Aldrich). The reaction was performed on ice and stopped after 1 h, 2 h, 3 h, and 16 h by adding 4x loading dye containing 10% SDS, 10mM β-mercaptoethanol, 20% glycerol, 0.2 M Tris, pH 6.8, 0.05% bromophenol blue. The samples from every time point were subjected to SDS-PAGE gel electrophoresis using a 15% acrylamide gel (Figure S9).

Bioactivity: In vivo characterization of TNFα was assessed based on cytotoxicity assays using mouse fibroblasts cells (LM L929, ATCC®) as previously described [24]. The fibroblast cells were seeded at 3.10^5 cells per well in a 96-well array and incubated at 37 °C for 24 h. Cell growth was inhibited using 1 µg/ml actinomycine D (Sigma Aldrich). The cells were incubated for 18h with a serial dilution ranging from 10 nM to 1 fM of TNFα, subsequently stained with 7 µl of CellTiter 96® AQues (Promega) at 37 °C for 2.5 h. The number of viable cells was measured by the absorbance at 490 nm, and results are given in comparison to cells treated with actinomycine D only. Duplicates of the 8 dilution points were measured. Buffer background absorbance, based on buffer samples, at 650 nm was subtracted. The data were fitted using the equation y = m1+(m2-m1)/(1+(x/m3)^m4) (cf. KaleidaGraph) [25]. To increase the robustness of the fit, m2 was fixed to zero, m1 and m4 were fitted globally overall all the datasets and solely m3 adjusted independently for each dataset (Figure S10).

Supporting Figures

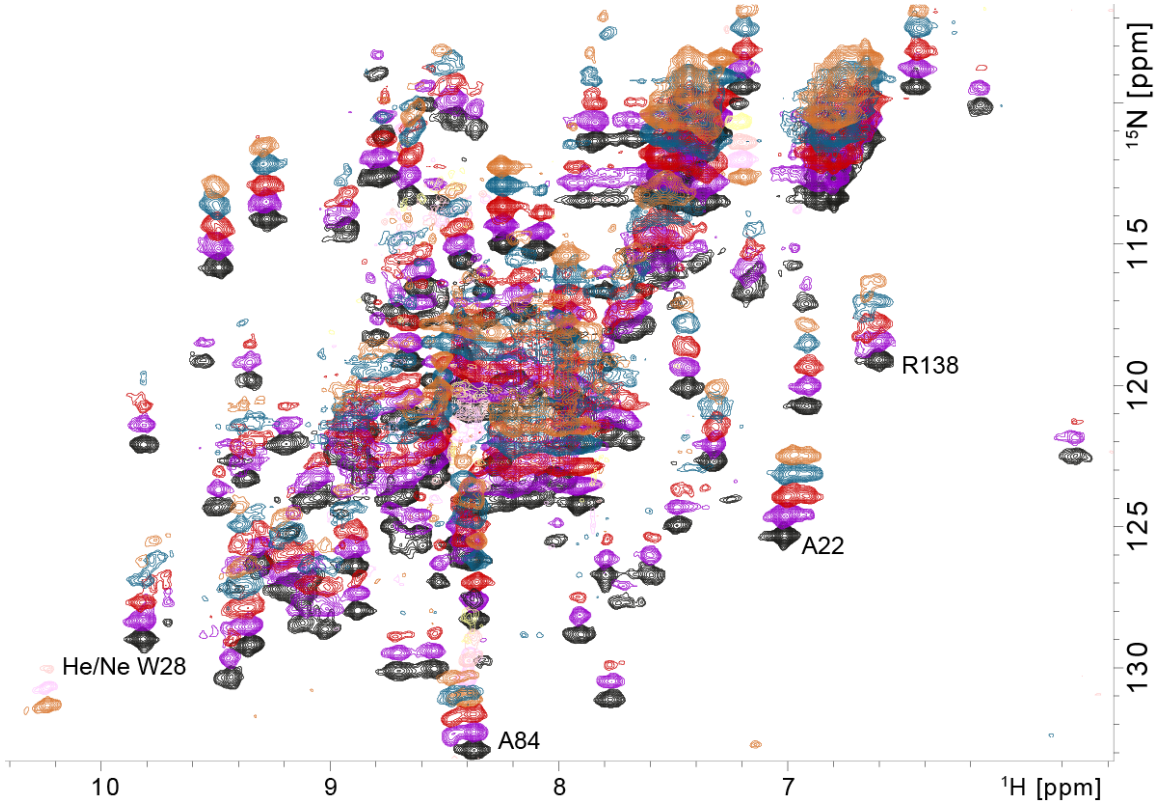

Figure S1. Full spectrum of Figure 3D in the main text. Residues mentioned in the main text are labeled with their residue number and amino acid type.

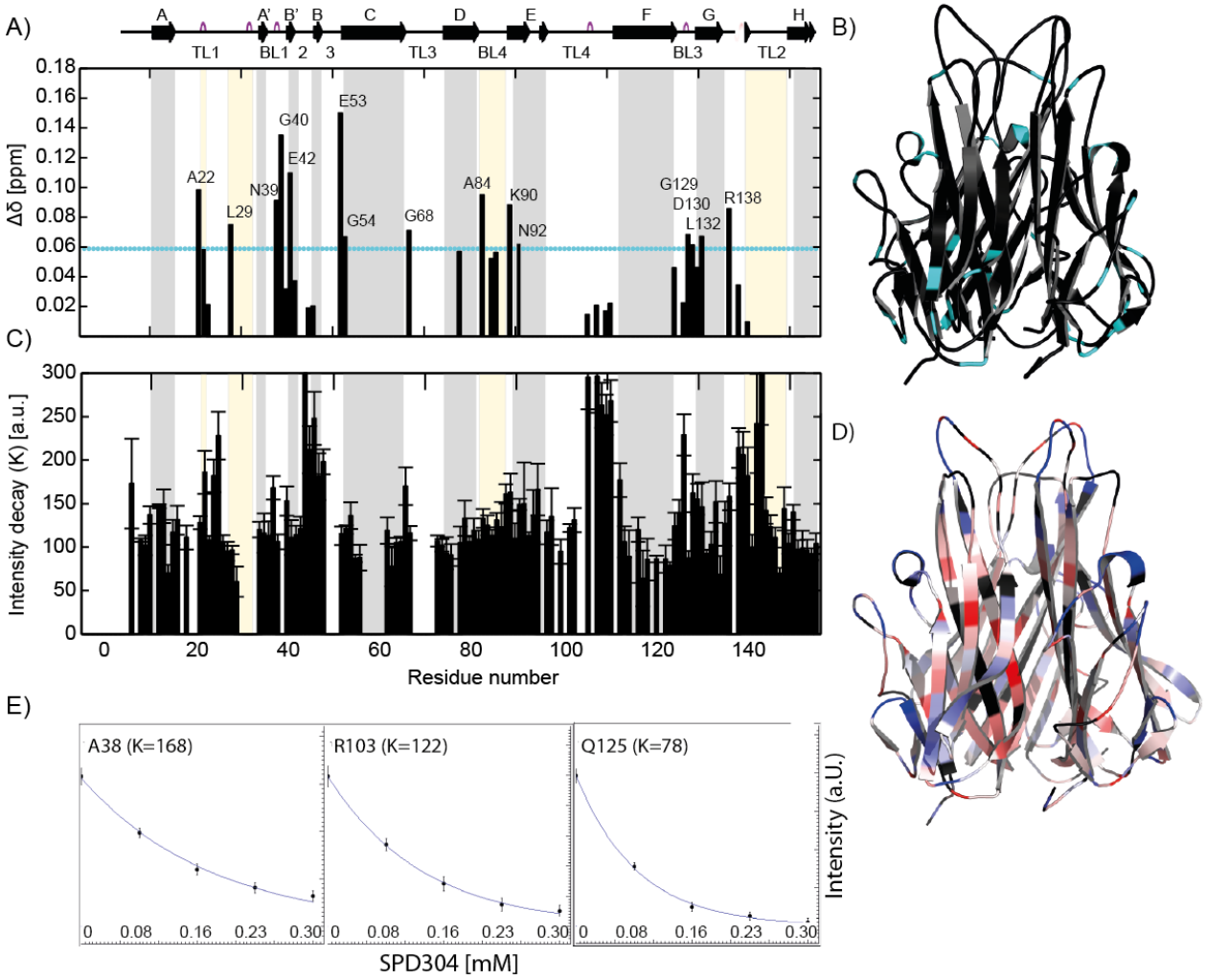

Figure S2. SPD304 induces conformational exchange at the PPI and at the mediating receptor interaction site. A) Combined chemical shift perturbation (Δδ) for the backbone ^{1}H and ^{15}N resonances (chemical shifts submitted to BMRB data base (access code 27266)), between TNFα and TNFα:SPD304 (1:1.4). Spectra were recorded at 600 MHz, 310 K using a 230 μM ^{15}N-labled protein sample. Signals, which could not be unambiguously followed due to severe exchange broadening or overlap, were excluded. Residues being part of secondary structure motives [4] are colored in gray, residues mediating receptor interaction in yellow [26,27]. B) Resonances with a higher than average Δδ (horizontal cyan line in A)) are mapped on the crystal structure (cyan). C) Decrease in resonance intensities, $I_{[SPD304]}$, upon interaction with SPD304, characterized using the decay constant K obtained from fitting to an exponential decay $I_{[SPD304]} = I_0 \cdot \exp(-[SPD304]/K)$ with I_0 the initial peak intensity (see Supporting Methods). Color-coding as in (A). D) K is plotted on the crystal structure (PDB:1TNF) using a red-white-blue color code (red = large change (K=50) and blue = small change (K=200). E) Data from three residues illustrating the exponential decay in signal intensity due to increasing amounts of SPD304. The residue whose data is shown is indicated in the top left corner and the intensity decay constant is given in brackets.

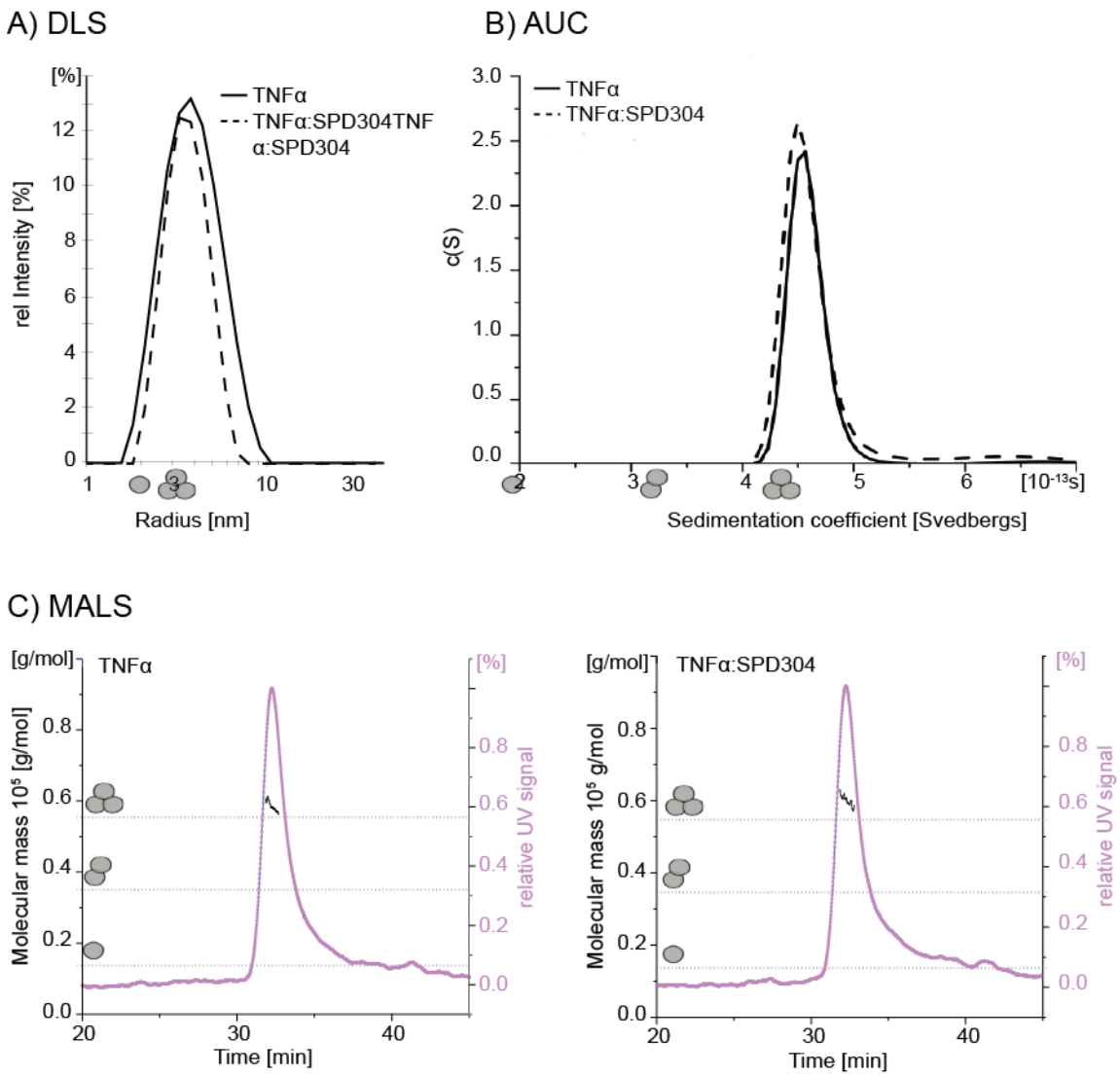

Figure S3. Evidence for retention of the trimeric state of TNFα in presence of SPD304. The interaction was assumed to be strong (µM), as published [28]. A-C) Values expected for a monomer, dimer, or trimer assuming a spherical molecule are indicated in the graphs with the corresponding number of gray spheres. A) DLS was measured with TNFα (solid line) and TNFα:SPD304 (1:5) (dashed line). Triplicates of measurements were averaged. B) AUC was performed with TNFα (solid line) and TNFα:SPD304 (1:7) (dashed line). C) SEC coupled to MALS measurements were performed with TNFα and TNFα:SPD304 (1:3). The samples were resolved on the column. The molecular mass, based on the scattering of the two samples is shown in black. Please note, the size of the trimer is slightly decreasing across the UV absorbance peak.

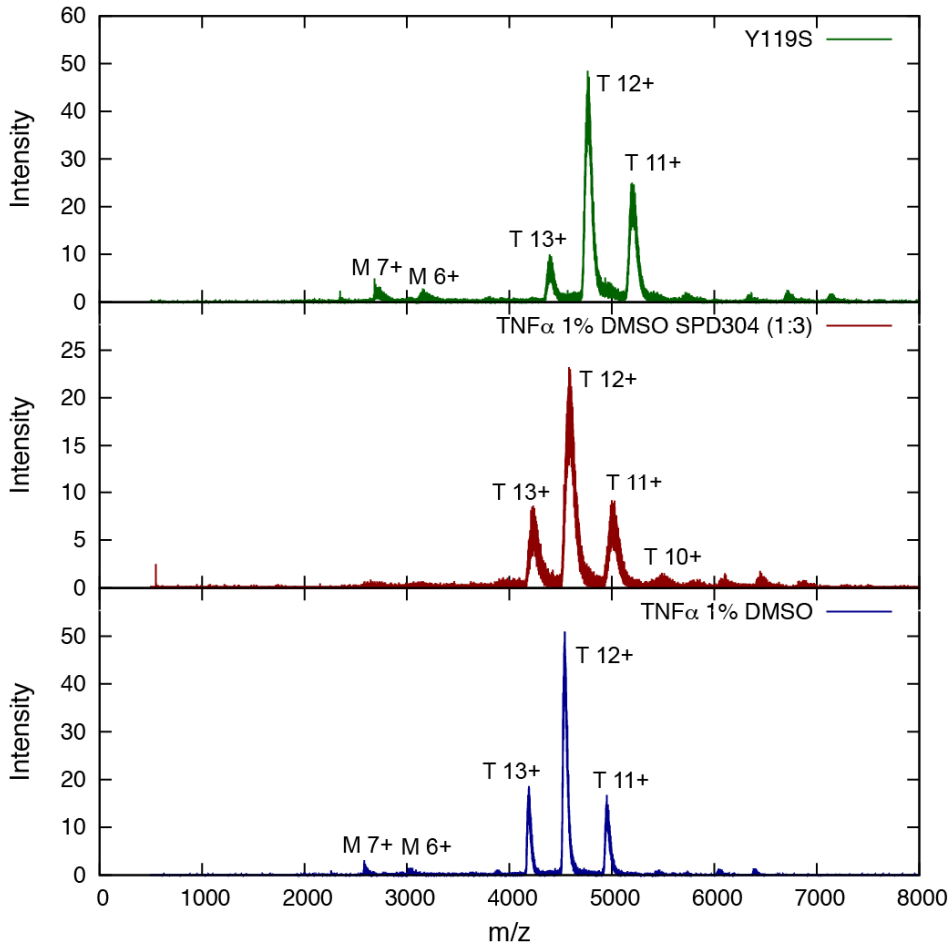

Figure S4. Interaction between TNFα and SPD304 and the trimeric nature of active and inactive TNFα forms. NanoESI mass spectra of TNFα (4.5 μM) (bottom), TNFα in presence of SPD304 (TNFα 4.5 μM, SPD304 13.5 μM) (middle), and the mutant Y119S (4.5 μM) (top). The Y119S mutant was uniformly labeled with ^{15}N and ^{13}C isotopes, explaining the shift to higher m/z in the observed signals. The letter 'T' marks peaks corresponding to trimeric TNFα and charge states are indicated; 'M' denotes small amounts of monomeric TNFα.

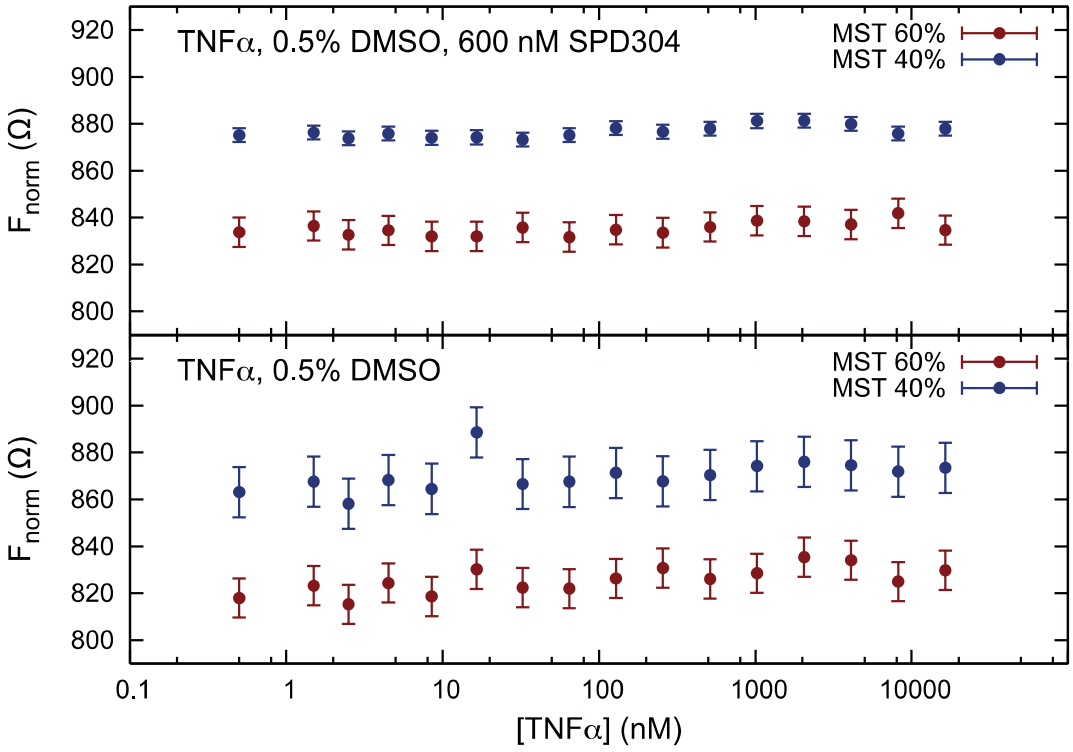

Figure S5. MicroScale thermophoresis (MST) of fluorescently labeled TNFα alone or in presence of SPD304. The MST signals (F_{norm}) of 0.5nM of fluorescently labeled TNFα was monitored upon addition of unlabeled TNFα up to the indicated concentration in presence (top) and in absence (bottom) of SPD304 (600 nM). Assuming a K_D between TNFα and SPD304 of ~5 μM [29], 95% and 50% of TNFα is saturated at protein concentrations up to 250 nM and 4 μM, respectively. The MST was measured using 40% (blue dots) and 60% (red dots) MST power. The presented results are averaged over duplicate experiments. No significant change in thermophoresis was observable. This is in accordance with the expectation that TNFα in presence or absence of SPD304 retains its trimeric state in the nM to mM concentration range.

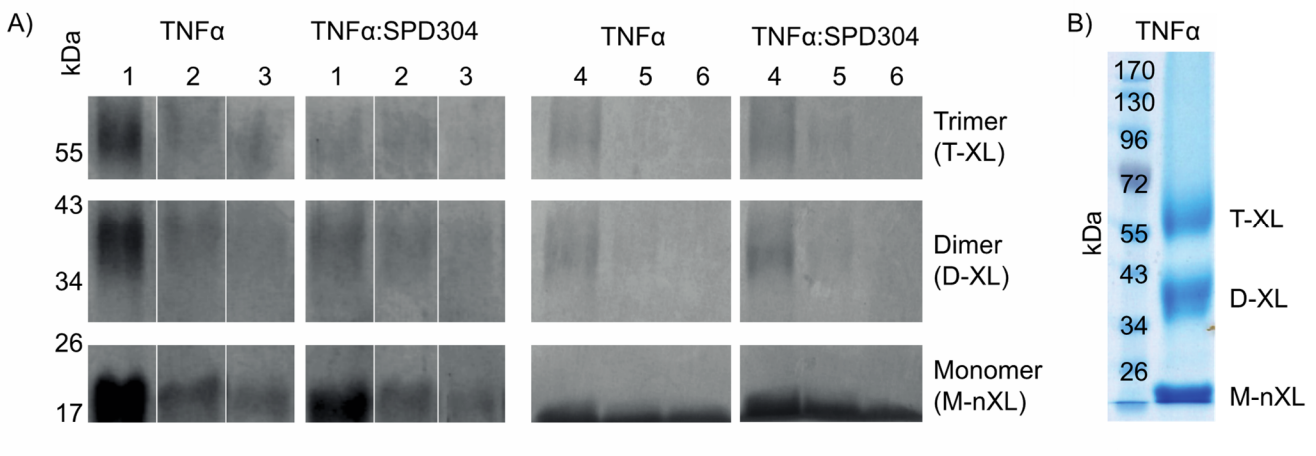

Figure S6. TNFα forms trimers that can be cross-linked at high nM concentrations both in presence and absence of SPD304. A) TNFα and TNFα:SPD304 (1:100) samples were prepared at concentrations of 5 µM (lane 1), 500 nM (lane 2), 50 nM (lane 3) as well as 1 µM (lane 4), 100 nM (lane 5) and 10 nM (lane 6) and cross-linked using DMTMM and PHD [23]. The reaction was resolved and visualized on an SDS-PAGE (15% acrylamide) gel followed by silver staining. Trimeric (T-XL) and dimeric (D-XL) cross-linked species as well as monomeric (M-nXL) forms are observable. B) No larger oligomeric species than trimers are produced by cross-linking.

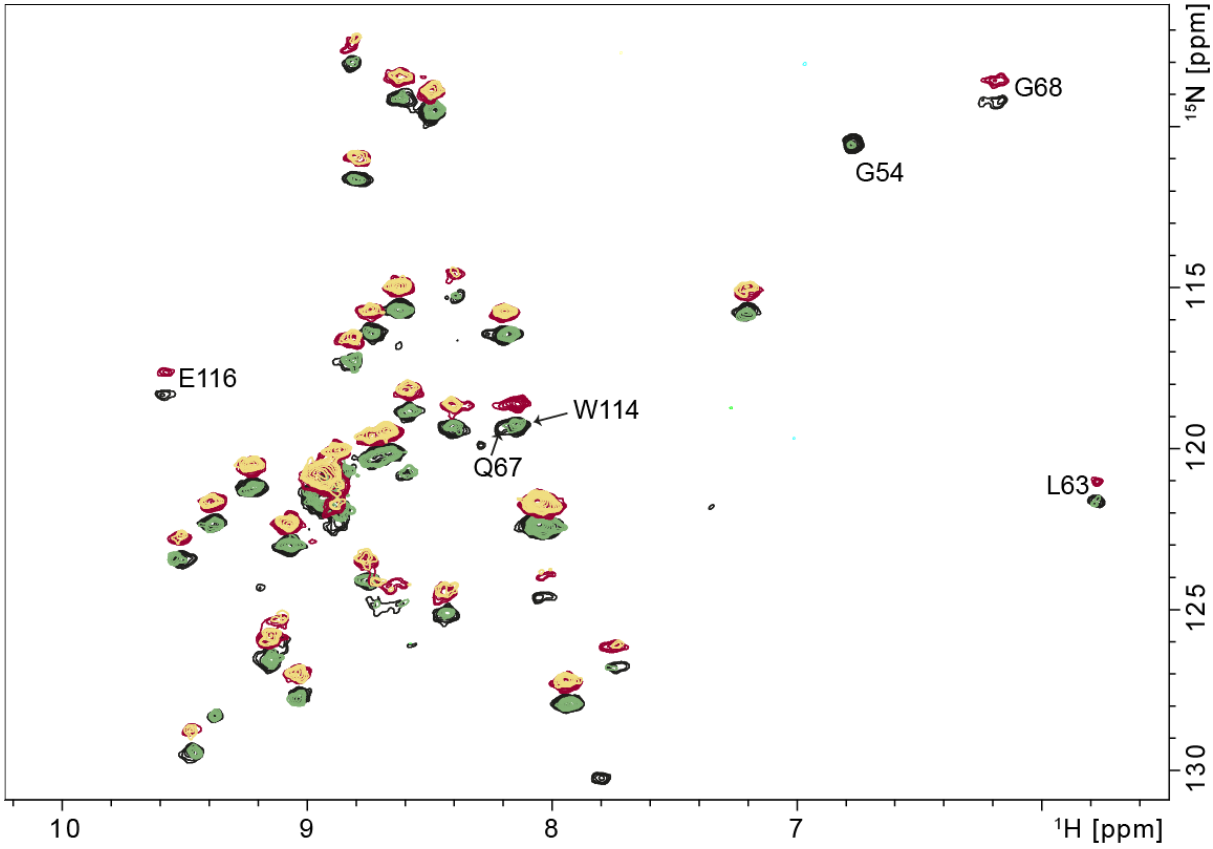

Figure S7. Quenched H/D exchange experiments confirming the retention of the secondary structure for the TNFα:SPD304 complex. [^{1}H, ^{15}N]-HSQC spectra were measured after 10 min of exchange in 100% D_2O in absence (black) or presence (green) of SPD304 and after 4h of exchange in 100% D_2O in absence (red) or presence (yellow) of SPD304 (see Supporting Methods). The spectra after 4h are shifted with a small offset of 0.6 ppm in the ^{15}N dimension for better visibility. Residues showing altered H/D exchange phenomena are labeled. These residues all cluster at the top of the inner β-sheets C and F.

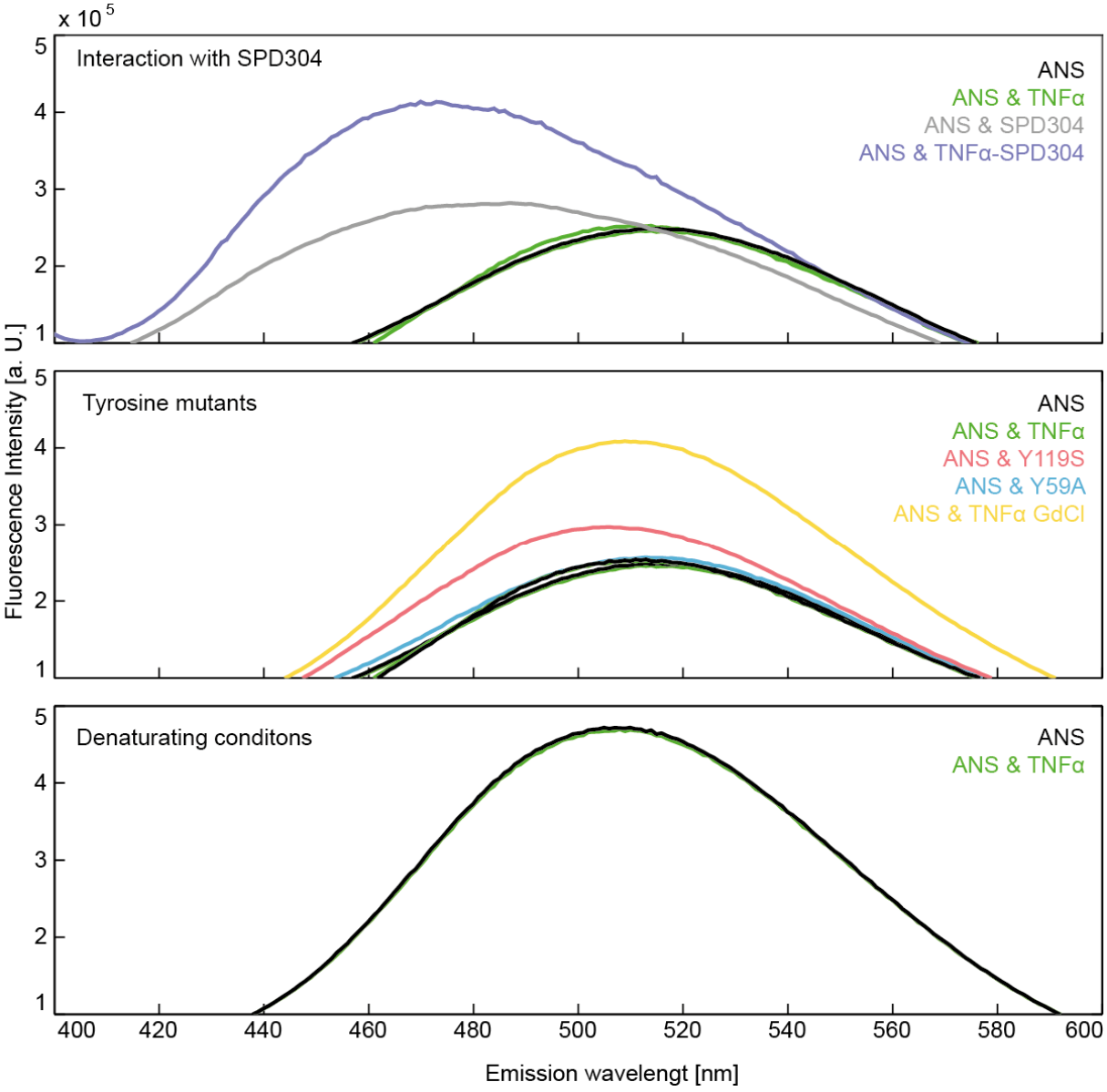

Figure S8. "Molten globular like" characteristics for TNFα by interaction with the hydrophobic fluorescent probe ANS. All measurements were conducted at 30 °C, ANS was excited at 380 nm and the fluorescence was detected between 400 and 600 nm, plotted in arbitrary units. ANS fluorescence in presence of TNFα or SPD304 (top), in presence of TNFα, Y119S or Y59A mutants (middle) or in presence of TNFα under denaturing conditions: 8M urea, 2 mM DTT (bottom). Color coding: ANS (black), ANS and TNFα (green), ANS and SPD304 (grey), ANS and TNFα:SPD304 (1:4.6) (violet), ANS and TNFα Y119S (red), ANS and TNFα Y59A (cyan) and ANS and TNFα in presence of 1 M GdCl (yellow). Upon interaction with SPD304, the fluorescence maximum increases for TNFα:SP304 and for the mutant Y119S and shifts slightly towards larger wavelengths. Maximal increase in fluorescence was estimated using TNFα in presence of 1 M GdCl, which is known to induce a molten globular state for TNFα [30,31]. ANS does not bind to unfolded TNFα (bottom) as expected [32].

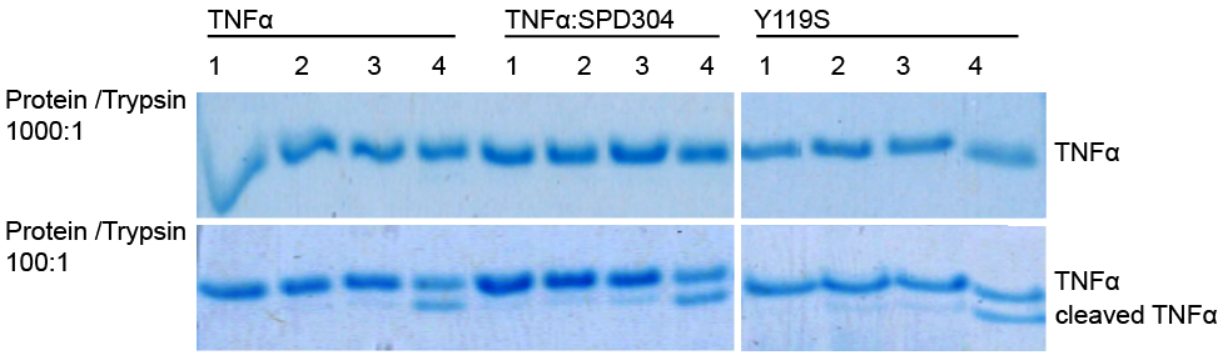

Figure S9. Probing structural modification in the receptor-binding site Top loop 1 (TL1, Figure 1A) for PPI-perturbed TNFα using trypsin cleavage at the RRA sequence. TNFα, TNFα:SPD304 (1:1) and Y119S were mixed with Trypsin in a (top) 1000:1 or (bottom) 100:1 (w/w) ratio. The samples were submitted to 1 h (1), 2 h (2), 3 h (3) and 16 h (4) of trypsin digestion and analyzed on a 15% SDS-PAGE gel. The two observable bands correspond to monomeric full length TNFα (6-157) at approximately 17 kDa and trypsin digested cleaved TNFα [33].

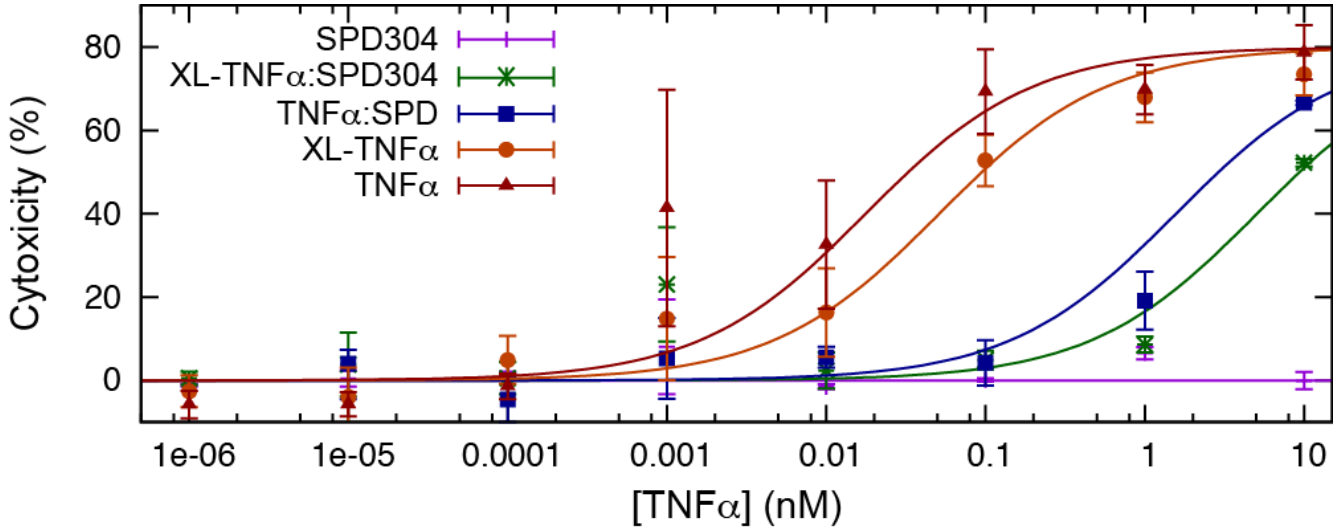

Figure S10. *In vivo* activity of TNFα measured by cytotoxic assay using mouse fibroblast cells. Each point describes the mean value (standard deviations are indicated as coarse estimations of the errors) of duplicates of mouse fibroblast L9292 cells viability ($A_{490\,nm}$ - $A_{650\,nm}$) for different TNFα concentrations in the presence of 1 µg/ml actinomycine D. Estimated IC_{50} values are 0.05 nM, 0.02 nM, 1.6 nM, and 5.1 nM, for TNFα, XL-TNFα, TNFα:SPD304, and XL-TNFα:SPD304, respectively. Cross-linked TNFα:SPD304 (1:100) has reduced bioactivity compared to TNFα, also when cross-linked.

Supporting Tables

Table S1. Comparison of the intensity decay[1] in NMR spectra of different PPI-perturbed TNFα.

	Interface mutants				*Non-interface mutants*		
	L57Y	*Y59A*	*Y119S*	*G121A*	*T72A*	*T89A*	*I97A*
R[2]	0.1886	0.703	0.424	0.563	-0.177	-0264	-1.350
P[2]	0.0821	0.000	0.000	0.000	0.130	0.0138	0.215

[1] The relative intensity change of TNFα:SPD304 (1:1) was compared with the different TNFα-mutants L57Y, Y59A, Y119S, G121A, T72A, T89A, I97A.

[2] Pearson correlation coefficients (R) and p-values (P) testing against no relationship using a 95% confidence interval are given. This reveals high to moderate correlation between interface mutants and the complex TNFα:SPD304, but no correlation with non-interface mutants.

Table S2. SEC analysis of different forms of TNFα[1]

	TNFα		*Interface mutants*				*Non-interface mutants*		
	TNFα	*TNFα:SPD304*[2]	*Y59*	*G121*	*Y119*	*L57*	*T89*	*T72*	*I97*
V_{ret} [mL] [2,3]	11.15	11.1	11.3	10.9	11.5	11.4	11.1	11.4	11.0

[1] Free, mutant TNFα, and TNFα:SPD304 complex (1:1.4).

[2] The similar values for the retention volume (V_{ret}) confirm the preservation of the trimeric state.

[3] An error of ±0.25 mL was determined for TNFα and is expected to be similar for the other measurements.

Table S3. DLS analysis of different forms of TNFα[1]

	TNFα	*Y119S*	*TNFα:SPD304*
H_D [nm] [2]	6.5±1.5	6.5±1.9	6.4±1.4

[1] TNFα, mutant Y119S (most disrupting) as well as for the TNFα:SPD304 complex (1:5).

[2] The similar values for the hydrodynamic diameter (H_D) confirm the preservation of the trimeric state.

Table S4. Structural characteristics for different forms of TNFα[1] for residues involved in receptor-binding[2].

Loop residue	*HSQC[3] TNFα*	*NOE[4] TNFα*	*η_{xy} [s^{-1}][5] TNFα*	*HSQC[3] TNFα-SPD304*	*NOE[4] TNFα-SPD304*	*η_{xy} [s^{-1}][5] TNFα-SPD304*	*HSQC[3] Y119S*	*NOE[4] Y119S*
				TL1				
E23	resolved[6]	Q21 / A22		double[7] overlap[9]	no change[8]	13.83 ±1.21	double	no change
L29	resolved	A18/V19	21.57 ±0.73	double	no change	29.23 ±0.71	double	no change
N30	resolved			overlap			overlap	overlap
R31	-							
R32	-			-			-	
				TL2				
D143	resolved	F144	-	shifted [10]		-	-	-
F144	resolved	A145/D143	21.72 ±0.85	overlap		-	overlap	
A145	resolved	F144	24.88 ±0.30	overlap			shifted	no change
E146	overlap	-						
S147	overlap	-						
G148	resolved	Q149	19.69 ±0.93	-		-	shifted	no change
Q149	resolved	G148 V150	27.21 ±0.44	-		-	shifted	no change
				BL4				
A84	resolved	I83/V85/	29.23 ±3.04	double	No change	28.55 ±4.38	double	no change
V85	resolved	A84/	25.93 ±0.40	overlap			overlap	
S86	resolved	-	23.52 ±1.92	double	-	28.13 ±4.56	double	
Y87	resolved	-	18.91 ±2.36	double	-	24.40 ±1.74	double	
Q88	overlap	-						
T89	overlap NH2	A84 (4.4)						
K90	resolved	V91	22.91 ±1.18	double	no change	26.53 ±1.78	double	no change
V91	resolved	R82	31.16 ±2.0	-			-	

[1] TNFα, Y119S mutant, and TNFα:SPD304.

[2] Details for every experiment are given in Supporting Methods.

[3] ^{1}H-^{15}N resonances in the HSQC spectra.

[4] Observed [^{1}H,^{1}H]-[^{1}H-^{15}N]-NOE pattern.

[5] Cross-correlated relaxation rate η_{xy}.

[6] Only resolved resonances are analyzed which are separated from any other resonance by at least 0.06 ppm in ^{1}H and 0.6 ppm and in ^{15}N frequencies.

[7] Double refers to either a change in resonance shape or the appearance of a second or multiple resonance(s) in close proximity.

[8] No change means; the identical NOE pattern is observed as compared to TNFα.

[9] Overlap refers to ambiguity in the assignments.

[10] Shifted refers to a change in ^{1}H and/or ^{15}N frequency (Supporting Figure S2); chemical shifts were submitted to the BMRB database (access code 27266).

REFERENCES

(1) Cubrilovic, D.; Barylyuk, K.; Hofmann, D.; Walczak, M. J.; Gräber, M.; Berg, T.; Wider, G.; Zenobi, R. *Chem. Sci.* **2014**, *5*, 2794.

(2) Krishnarjuna, B.; Jaipuria, G.; Thakur, A.; D'Silva, P.; Atreya, H. S. *J. Biomol. NMR* **2011**, *49*, 39.

(3) Corti, A.; Poiesi, C.; Merli, S.; Cassani, G. *J. Immunol. Methods* **1994**, *177*, 191.

(4) Eck, M. J.; Sprang, S. R. *J. Biol. Chem.* **1989**, *264*, 17595.

(5) Wishart, D. S.; Sykes, B. D. *J. Biomol. NMR* **1994**, *4*, 171.

(6) Farrow, N. A.; Zhang, O.; Forman-Kay, J. D.; Kay, L. E. *J. Biomol. NMR* **1994**, *4*, 727.

(7) Kay, L. E.; Torchia, D. A.; Bax, A. *Biochemistry* **1989**, *28*, 8972.

(8) Dosset, P.; Hus, J. C.; Blackledge, M.; Marion, D. *J. Biomol. NMR* **2000**, *16*, 23.

(9) Lipari, G.; Szabo, A. *J. Am. Chem. Soc.* **1982**, *104*, 4546.

(10) Lipari, G.; Szabo, A. *J. Am. Chem. Soc.* **1982**, *104*, 4559.

(11) Clore, G. M.; Szabo, A.; Bax, A.; Kay, L. E.; Driscoll, P. C.; Gronenborn, A. M. *J. Am. Chem. Soc.* **1990**, *112*, 4989.

(12) Tjandra, N.; Szabo, A.; Bax, A. *J. Am. Chem. Soc.* **1996**, *118*, 6986.

(13) Wider, G.; Dreier, L. *J. Am. Chem. Soc.* **2006**, *128*, 2571.

(14) Williamson, M. P. *Prog. NMR Spectrosc*. **2013**, *73*, 1.

(15) Lee, D.; Hilty, C.; Wider, G.; Wüthrich, K. *J. Magn. Reson.* **2006**, *178*, 72.

(16) Hiyama, Y.; Niu, C.; Silverton, J. V; Bavoso, A. *J. Am. Chem. Soc.* **1988**, *110*, 2378.

(17) Whitmore, L.; Wallace, B. A. *Biopolymers* **2008**, *89*, 392.

(18) Wingfield, P.; Pain, R. H.; Craig, S. *FEBS Lett.* **1987**, *211*, 179.

(19) Hlodan, R.; H. Pain, R. *FEBS Lett.* **1994**, *343*, 256.

(20) Sawicki, M. *Publ. Astron. Soc. Pacific* **2012**, *124*, 1208.

(21) Scotti, A.; Liu, W.; Hyatt, J. S.; Herman, E. S.; Choi, H. S.; Kim, J. W.; Lyon, L. A.; Gasser, U.; Fernandez-Nieves, A. *J. Chem. Phys.* **2015**, *142*, 234905.

(22) Niesen, F. H.; Berglund, H.; Vedadi, M. *Nat. Protoc.* **2007**, *2*, 2212.

(23) Leitner, A.; Joachimiak, L. A.; Unverdorben, P.; Walzthoeni, T.; Frydman, J.; Förster, F.; Aebersold, R. *Proc. Natl. Acad. Sci.* **2014**, *111*, 9455.

(24) Chiu, W. C.; Lai, Y. P.; Chou, M. Y. *PLoS One* **2011**, *6*, 16373.

(25) DeLean, A.; Munson, P. J.; Rodbard, D. *Am. J. Physiol.* **1978**, *235*, 97.

(26) Mukai, Y.; Shibata, H.; Nakamura, T.; Yoshioka, Y.; Abe, Y.; Nomura, T.; Taniai, M.; Ohta, T.; Ikemizu, S.; Nakagawa, S.; Tsunoda, S. ichi; Kamada, H.; Yamagata, Y.; Tsutsumi, Y. *J. Mol. Biol.* **2009**, *385*, 1221.

(27) Mukai, Y.; Nakamura, T.; Yoshikawa, M.; Yoshioka, Y.; Tsunoda, S.; Nakagawa, S.; Yamagata, Y.; Tsutsumi, Y. *Sci. Signal.* **2010**, *3*, 83.

(28) He, M. M.; Smith, A. S.; Oslob, J. D.; Flanagan, W. M.; Braisted, A. C.; Whitty, A.; Cancilla, M. T.; Wang, J.; Lugovskoy, A. a; Yoburn, J. C.; Fung, A. D.; Farrington, G.; Eldredge, J. K.; Day, E. S.; Cruz, L. a; Cachero, T. G.; Miller, S. K.; Friedman, J. E.; Choong, I. C.; Cunningham, B. C. *Science* **2005**, *310*, 1022.

(29) Melagraki, G.; Ntougkos, E.; Rinotas, V.; Papaneophytou, C.; Leonis, G.; Mavromoustakos, T.; Kontopidis, G.; Douni, E.; Afantitis, A.; Kollias, G. *PLoS Comput. Biol.* **2017**, *13*, 1005372.

(30) Kim, Y. R.; Hahn, J. S.; Hong, H.; Jeong, W.; Song, N. W.; Shin, H. C.; Kim, D. *Biochim. Biophys. Acta* **1999**, *1429*, 486.

(31) Hlodan, R.; Pain, R. H. *Eur. J. Biochem.* **1995**, *231*, 381.

(32) Semisotnov, G. V.; Rodionova, N. A.; Razgulyaev, O. I.; Uversky, V. N.; Gripas', A. F.; Gilmanshin, R. I. *Biopolymers* **1991**, *31*, 119.

(33) Cha, S. S.; Kim, J. S.; Cho, H. S.; Shin, N. K.; Jeong, W.; Shin, H. C.; Kim, Y. J.; Hahn, J. H.; Oh, B. H. *J. Biol. Chem.* **1998**, *273*, 2153.